Effect of Temperature on the Structure of Trout Troponin C[†]

Tharin M. A. Blumenschein,[‡] Todd E. Gillis,[§] Glen F. Tibbits,[§,||] and Brian D. Sykes*[,‡]

CIHR Group in Structure and Function and Department of Biochemistry, University of Alberta, Edmonton, Alberta, Canada T6G 2H7, Department of Biological Sciences and Cardiac Membrane Research Lab, Simon Fraser University, Burnaby, British Columbia, Canada V5A 1S6, and Cardiovascular Sciences, British Columbia Research Institute for Children's and Women's Health, Vancouver, British Columbia, Canada V5Z 4H4

Received August 21, 2003; Revised Manuscript Received January 30, 2004

ABSTRACT: Adaptation for life at different temperatures can cause changes in many aspects of an organism. One example is the expression of different protein isoforms in species adapted to different temperatures. The calcium regulatory protein cardiac troponin C (cTnC), from rainbow trout (*Oncorhynchus mykiss*), is a good model for studying temperature effects, both because of its low physiological temperature and because mammalian cTnC, extensively studied at higher temperatures, can be used for comparison. We determined the structure and studied the backbone dynamics of the regulatory domain of trout cardiac troponin C (ScNTnC) with one Ca^{2+} bound at 7 and 30 °C, using nuclear magnetic resonance spectroscopy (NMR). The overall fold of the regulatory domain of trout cTnC at both temperatures is similar to the regulatory domain of mammalian (human, bovine, and porcine isoform) cTnC bound to one Ca^{2+}. By comparing the trout structures at the two temperatures, we identify differences between the positions of the helices flanking the calcium binding loops, and the overall structure at 7 °C is more compact than that at 30 °C. The structure at 7 °C is more similar to the mammalian cTnC, which was determined at 30 °C, indicating that they have the same conformation at their respective physiological temperatures. The dynamic properties of the regulatory domain of trout cTnC are similar at the two temperatures that were used in these studies.

Life exists over a wide range of temperatures, requiring adaptations of biological processes to function at high- and low-temperature extremes. These adaptations occur at different levels, from macroscopic structures to changes in protein sequences and conformations. Many proteins are known to have different isoforms in organisms that live at different temperatures; these proteins often have different thermostabilities and are active at different temperatures, according to the physiological temperatures in each organism (*1*). However, not many proteins have had their tertiary structures determined at more than one temperature, and it is therefore difficult to determine a priori the effect of temperature on the conformation of different isoforms.

The global effect of temperature changes on proteins has been studied for a number of properties, including thermal denaturation, compressibility, and volume (for examples, see refs *1*−*11*). Proteins from organisms that live at higher temperatures are typically more resistant to thermal denaturation, and protein volume tends to increase with the increase in temperature. As the temperature increases, proteins undergo anisotropic expansion, and the average distance between its atoms increases (*5*, *8*−*11*).

Compared to the relatively high temperature of mammals, trout and other temperate fish live in colder and more variable temperatures. This requires adaptations at various levels. For instance, the trout heart normally functions at low (4−8 °C) temperatures, while mammalian hearts are not functional at the same temperatures. One important aspect of this observation is that the Ca^{2+} affinity of the cardiac contractile element of all species examined to date diminishes dramatically as the temperature decreases. The compensating adaptation has been shown to be to a significant (>200%) increase in the Ca^{2+} affinity of the cardiac contractile element of the trout in comparison to those of mammals over a broad range of temperatures. This is due, at least in part, to effects of temperature on the calcium regulatory protein, cardiac troponin C (cTnC)[1] (*12*, *13*). When the intracellular levels of Ca^{2+} in the heart or skeletal muscle cells increase as a consequence of depolarization, TnC binds Ca^{2+} and undergoes conformational changes that are propagated to other proteins in the muscle, starting myofibril contraction (*14*).

[†] Supported by the Canadian Institutes of Health Research (CIHR), the Heart and Stroke Foundation of British Columbia and Yukon, and the Natural Sciences and Engineering Research Council of Canada (NSERC). T.M.A.B. is the recipient of an Alberta Heritage Foundation for Medical Research postdoctoral fellowship, and T.E.G. was the recipient of a doctoral fellowship from the Heart and Stroke Foundation of Canada.

* To whom correspondence should be addressed. Phone: (780) 492-5460. Fax: (780) 492-0886. E-mail: Brian.Sykes@ualberta.ca.

[‡] University of Alberta.

[§] Simon Fraser University.

[||] British Columbia Research Institute for Children's and Women's Health.

[1] Abbreviations: TnC, troponin C; TnI, troponin I; cTnC, cardiac troponin C; sTnC, skeletal troponin C; NTnC, N-terminal domain of troponin C; sNTnC, N-terminal domain of skeletal troponin C; ScNTnC, N-terminal domain of trout (salmonid) cardiac troponin C, residues 1−89; NMR, nuclear magnetic resonance spectroscopy; NOE, nuclear Overhauser effect; NOESY, NOE spectroscopy; HSQC, heteronuclear single-quantum coherence; rmsd, root-mean-square deviation; ASA, accessible surface area.

10.1021/bi035504z CCC: $27.50
Published on Web 04/07/2004

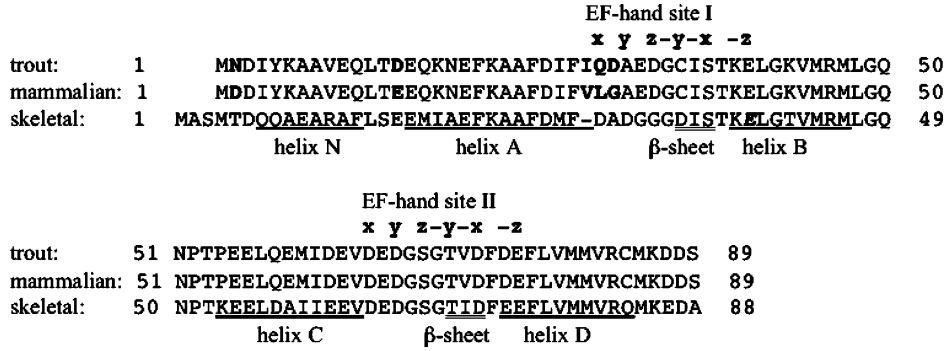

FIGURE 1: Sequence alignment of the regulatory (N-terminal) domain of troponin C (TnC), comparing trout cardiac TnC, mammalian (human, bovine, and porcine isoform) cardiac TnC, and chicken skeletal TnC. The differences between trout and mammalian cardiac TnC are shown in bold, and the position of the skeletal E41A mutation is shown in bold italics. The secondary structure features are underlined, and the Ca^{2+}-coordinating positions in each EF-hand site are shown above the sequences.

TnC is an EF-hand protein, containing two domains, each with two EF-hand metal binding sites. Each EF-hand site is composed of a 12-amino acid loop flanked by two α-helices. Six positions from the loop (1, 3, 5, 7, 9, and 12) are responsible for chelating the metal ion, either directly or indirectly (*15*). In TnC, the C-terminal domain both has high-affinity EF-hand sites permanently occupied by either Ca^{2+} or Mg^{2+} and is responsible for anchoring TnC to the rest of the troponin complex. The EF-hand sites in the N-terminal or regulatory domain are empty when the muscle is relaxed, but bind Ca^{2+} when the cytosolic concentrations increase, and trigger muscle contraction. Skeletal muscle TnC has two functional EF-hand sites in its N-terminal domain, while in mammalian cTnC, the first EF-hand site is defunct and unable to bind Ca^{2+} (*16*). In trout cardiac TnC, differences in the amino acids in positions 28−30 make the first EF-hand site capable of binding Ca^{2+}, but only at nonphysiological concentrations in the millimolar range (*17*). This makes it different from mammalian cTnC and similar to the E41A mutant of skeletal TnC, in which the glutamate in position 12 of the EF-hand site was replaced with an alanine, decreasing the Ca^{2+} affinity of site I (*18*). The sequences of the regulatory domain for the three isoforms (trout cardiac, mammalian cardiac, and chicken skeletal) are compared in Figure 1.

At temperatures ranging from 7 to 37 °C, trout cardiac TnC (ScTnC) has a higher affinity for Ca^{2+} than mammalian cTnC (*13*). This is also seen when only the N-terminal domain of each protein is used, despite the sequence similarities (only five differences in the 89 amino acids in the regulatory domain; see Figure 1) (*19*). Determining the structure and measuring the backbone dynamics of ScNTnC at two different temperatures, one corresponding to the trout physiological temperature (7 °C) and one closer to the mammalian physiological temperature (30 °C), and comparing these properties to mammalian cNTnC, previously determined at 30 °C (*20*, *21*), should give us some insights into how those five residues are responsible for the different temperature responses and calcium affinities.

MATERIALS AND METHODS

NMR Sample Preparation. Apo-[^{15}N]ScNTnC, expressed and purified as described previously (*17*), was dissolved in 550 μL of NMR buffer (100 mM KCl and 10 mM imidazole in a 90% H_2O/10% D_2O mixture, treated with Chelex 100 to remove metal contaminants). To this sample were added NaN_3 to a final concentration of 0.03%, dithiothreitol to a final concentration of 20 mM, and 2,2-dimethyl-2-silapentane-5-sulfonic acid to a final concentration of 0.2 mM. The pH of the sample was adjusted to 6.9 (meter reading uncorrected for ^{2}H isotope effects), and the solution was filtered using a centrifuge tube filter with 0.22 μm pores. Five hundred microliters of the sample was transferred into an NMR tube. Aliquots of a 100 mM $CaCl_2$ solution were added until the {^{1}H,^{15}N}-HSQC NMR spectra showed that site II was saturated with Ca^{2+}, but before site I started to bind Ca^{2+}. This titration was identical to the first part of the titrations described previously (*17*). The protein concentration was determined to be 1.34 mM by amino acid analysis in duplicate. For the ^{15}N-filtered NOESY experiments in 99% D_2O, the NMR sample was transferred to a microcentrifuge tube and lyophilized, and then resuspended in 500 μL of D_2O.

NMR Experiments for Structure Determination. The ^{1}H and ^{15}N NMR chemical shift assignments of the ScNTnC·Ca^{2+} complex were determined using two- and three-dimensional (2D and 3D, respectively) NMR experiments described in Table 1, and having as a guideline the chemical shift assignments of mammalian (human, bovine, and porcine isoform) cNTnC·Ca^{2+} complex previously reported by Spyracopoulos *et al.* (*20*). The suite of NMR spectra (see Table 1) were acquired at both 7 and 30 °C, on a Varian Unity 600 MHz or INOVA 800 MHz spectrometer, equipped with 5 mm triple-resonance probes and *z*-axis pulsed fields gradients for the 500 and 600 MHz instruments, and triple-axis gradients for the 800 MHz spectrometer. All experimental FIDs were processed using NMRPipe (*22*) and analyzed using NMRView (*23*). Generally, linear prediction for up to half the number of experimental points was used in indirect dimensions. Data were then zero-filled to the next power of 2, and typically multiplied by a sine-bell apodization function shifted by 60−90° before Fourier transformation.

Distance and Torsion Angle Restraints. Proton−proton distance restraints were derived from measured peak intensities in the NOESY spectra. Peaks from the 3D ^{15}N-edited NOESY-HSQC experiment were calibrated as previously described (*18*). Peaks from the 2D NOESY spectra were "binned" according to their integrated volume into three classes [strong (≤2.8 Å), medium (≤3.4 Å), and weak (≤5.0 Å)] using the internal calibration utility of NMRView (*23*). The minimum distance on all proton−proton restraints was set to 1.7 Å.

Table 1: NMR Experiments Used for Structure Determination

	nuclei[a]	^{1}H	nt[b]	*x*-pts[c]	*y*-pts[c]	*z*-pts[c]	*x*-sw[c]	*y*-sw[c]	*z*-sw[c]	mix[d]	ref
^{15}N HSQC	^{1}H, ^{15}N	600	24	1024	192	−	8000	1650	−	−	*39*
DIPSI-HSQC	^{1}H, ^{1}H, ^{15}N	600	16	1024	232	60	8000	5681	1650	−	*40*
^{15}N NOESY-HSQC	^{1}H, ^{1}H, ^{15}N	600	16	1024	248	64	8000	6579	1650	140	*40*
HNHA	^{1}H, ^{1}H, ^{15}N	600	8	1024	96	96	8000	4808	1650	−	*24*
HNHB	^{1}H, ^{1}H, ^{15}N	600	16	1024	128	64	8000	5000	1650	−	*26*
2D NOESY (in D_2O)	^{1}H, ^{1}H	800	32	8192	1024	−	9000	9000	−	100 (7 °C) 150 (30 °C)	*41*

[a] Nucleus acquired in each dimension, ordered as *x*, *y*, and *z*. [b] Number of transients acquired for each FID. [c] *x*-pts, *y*-pts, and *z*-pts are the number of complex points and *x*-sw, *y*-sw, and *z*-sw the sweep width in each dimension (*x* is the directly detected dimension). [d] Mixing times are given in milliseconds.

Table 2: Structural Statistics for ScNTnC·Ca^{2+}

	30 °C	7 °C
no. of NOE restraints		
total	1108	1249
intraresidue	471	506
sequential	317	359
medium-range ($\|i-j\| \leq 4$)	215	249
long-range ($\|i-j\| > 4$)	106	135
no. of dihedral restraints		
total	118	98
ϕ	51	50
ψ	50	35
χ_1	17	13
energies (kcal/mol)[a]		
E_{total}	141.4 ± 5.0	151.14 ± 3.9
$E_{dihedral}$	0.303 ± 0.132	0.237 ± 0.118
E_{NOE}	12.71 ± 1.54	11.21 ± 1.06
rmsd from the averaged structure (Å)[b]		
total	1.297 ± 0.086	1.242 ± 0.092
heavy atoms	1.120 ± 0.092	1.064 ± 0.093
backbone	0.677 ± 0.123	0.632 ± 0.112
$\phi-\psi$ in core or allowed regions[c] (%)		
residues in most favored regions	89.0	89.6
residues in additional allowed regions	10.3	9.1
residues in generously allowed regions	0.5	0.9
residues in disallowed regions	0.2	0.4
total volume (Å^3)	11450 ± 128	11200 ± 264
accessible surface area (ASA) (Å^2)	6118 ± 103	6005 ± 110
exposed nonpolar ASA (Å^2)	3125 ± 69	3050 ± 66

[a] Using all residues, for the lowest-energy structure. [b] Using residues 4−84. [c] Using all residues, as determined by Procheck (*30*).

Backbone ϕ dihedral angle restraints were obtained from $^3J_{HNH\alpha}$ coupling constants derived from the 3D HNHA spectrum (*24*). The peak intensities were assumed to have errors equal to the noise level, and the minimum restraint range was set to ±20°. Backbone ψ dihedral angle restraints were determined from the $d_{N\alpha}/d_{\alpha N}$ ratio (*25*). For $d_{N\alpha}/d_{\alpha N}$ ratios of >1.2, ψ was restricted to −30 ± 110°. For $d_{N\alpha}/d_{\alpha N}$ ratios of <0.71, ψ was restricted to −120 ± 100°. Restraints for some χ_1 angles were obtained from a 3D ^{15}N-edited HNHB spectrum (*26*).

Structure Calculations. Structures were generated with Xplor version 3.851 (*27*) using a simulated annealing protocol with 15 000 high-temperature steps and 9000 cooling steps, starting from an extended conformation, or 12 000 high-temperature steps and 6000 cooling steps, starting from the lowest-energy structure from the previous round of refinement to make calculations faster. The type and number of restraints that were used are summarized in Table 2. In later stages of the refinement process, six distance restraints of 2.0−2.8 Å to the Ca^{2+} ion in site II were added, based on homologous calcium binding sites (*28*). A few times during the refinement process, the calculation was started from an extended conformation, to check if the same results were obtained as when starting from the lowest-energy structure from the previous round. During each round, 60 structures were generated. Any NOE restraint that had violations larger than 0.2 Å was carefully checked. NOE and dihedral angle restraints were added gradually to the calculations. After the refinement was complete, the structures were checked using Vadar (*29*) and Procheck (*30*). The structural statistics presented in Table 2 are for the 40 lowest-energy structures from an ensemble of 60 structures. The atomic coordinates for both ensembles were deposited in the Protein Data Bank as entries 1R2U (30 °C) and 1R6P (7 °C). The chemical shifts were deposited in the BioMagResBank under accession number 5975.

Backbone Amide ^{15}N Relaxation Measurements and Analysis. The relaxation data were acquired at both 7 and 30 °C, on a Varian Unity 600 MHz spectrometer. Sensitivity-enhanced pulse sequences developed by Farrow *et al*. (*31*) were used to measure $^{15}N T_1$, $^{15}N T_2$, and {^{1}H}−^{15}N NOE values. $^{15}N T_1$ and $^{15}N T_2$ experiments were collected with 498 (t_1) × 96 (t_2) complex points; {^{1}H}−^{15}N NOE experiments were collected with 498 (t_1) × 64 (t_2) complex points. The T_1 relaxation delays were 11.1, 233.1, 466.2, 699.3, 932.4, 1165.5, and 1398.6 ms, and the delay between repetitions of the pulse sequence was 1.5 s. For T_2, the relaxation delays were 16.54, 49.63, 82.72, 115.8, 148.9, and 181.99 ms, and the delay between repetitions of the pulse sequence was set to 2 s. {^{1}H}−^{15}N NOEs were measured in the absence and presence of proton saturation. The period of ^{1}H saturation was 3 s, and the delay between repetitions of the pulse sequence in the presence of proton saturation was 2 s. In the absence of proton saturation, the delay between repetitions of the pulse sequence was 5 s. All relaxation data were processed with NMRPipe (*22*) (as described for the experiments used for structure determination) and analyzed with NMRView (*23*).

$^{15}N T_1$ and $^{15}N T_2$ relaxation data were fitted to a two-parameter exponential decay using the "Rate Analysis" function in NMRView. The error bars were obtained from the confidence intervals calculated by NMRView, using the standard deviation of the data from the fitted line as an estimate for the standard deviation in intensity. Uncertainties in the {^{1}H}−^{15}N NOE values were estimated from the baseplane noise in the {^{1}H,^{15}N}-HSQC spectra with and without proton saturation.

The order parameter S^2 was calculated for each residue as described previously (*32*). Briefly, backbone amide ^{15}N relaxation data were interpreted using the Lipari−Szabo model-free approach. The overall rotational tumbling of the

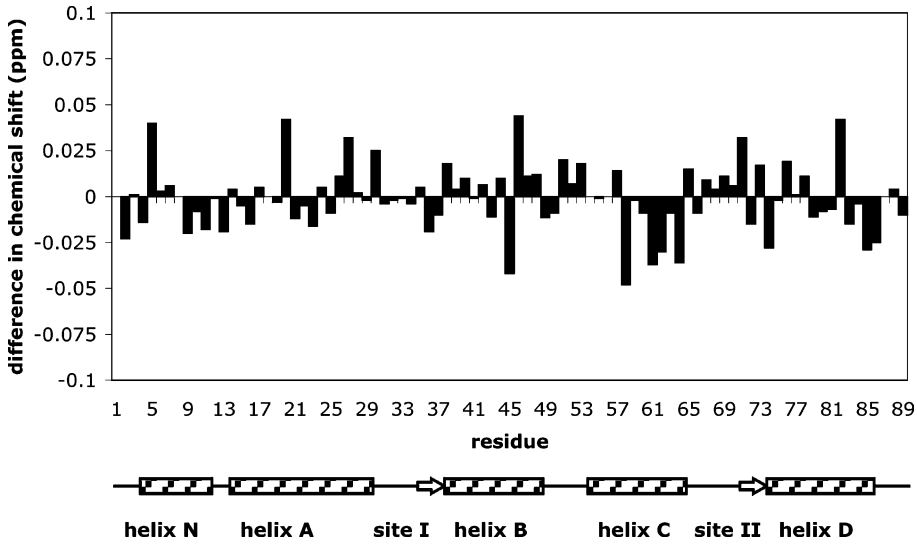

FIGURE 2: Differences in ^{1}H NMR chemical shift for H_α resonances as the temperature is decreased from 30 to 7 °C ($\delta_7 - \delta_{30}$). The largest changes are seen for residues 5, 20, 45, 46, 58, 61, 64, and 82. The changes seen here are much smaller than those observed for skeletal apo-TnC (*34*).

molecule was assumed to be isotropic, since mammalian cNTnC was shown to be isotropic to a first approximation (*21*), and given the similarity between the structures of trout and mammalian cNTnC. The experimental backbone amide relaxation parameters for each residue were fit using five different models for the spectral density function ($S^2-\tau_m$, $S^2-\tau_m-\tau_e$, $S^2-\tau_m-R_{ex}$, $S^2-\tau_m-\tau_e-R_{ex}$, and a two-time scale model). The fit was done using TENSOR version 2.0 (*33*), and the simplest model capable of fitting the data was used for each residue. For the fitting of S^2, the errors of T_1 and T_2 were fixed to 4%, which is closer to the actual experimental accuracy than errors derived from nonlinear least-squares fits.

RESULTS

To determine the structure of the ScNTnC·Ca^{2+} complex at 7 and 30 °C, a series of NMR experiments (Table 1) were carried out at each temperature. ^{1}H and ^{15}N NMR chemical shifts were assigned using those spectra, and the assignments of the mammalian (human, bovine, and porcine isoform) cNTnC·Ca^{2+} complex (*20*) as a guideline. Compared to the spectrum at 30 °C, {^{1}H,^{15}N}-HSQC cross-peaks at 7 °C were slightly shifted to lower field in both dimensions. In peptides, amide ^{1}H NMR chemical shift changes with temperature are typically linear, and the slope gives the temperature coefficient ($-\Delta\delta_{HN}/\Delta T$). The temperature coefficients for ScNTnC were presented when we described Ca^{2+} titrations at both temperatures (*17*). The cross-peaks in the NMR spectra were slightly broadened with the reduction in temperature, because the peak line width is proportional to the viscosity divided by the temperature (η/T) of the solution. The ^{1}H NMR chemical shift changes in the H_α proton resonance are a good indicator of changes in the secondary structure. Figure 2 displays the H_α chemical shift changes that occurred with a decrease in the temperature from 30 to 7 °C ($\delta_7 - \delta_{30}$). All the changes are fairly small, smaller than 0.05 ppm, and were upfield or downfield. The small size of the changes measured for the ScNTnC·Ca^{2+} complex makes it unlikely that they represent any significant change in its secondary structure.

The experimental distance and angle restraints derived from NMR are summarized in Table 2. The distribution of NOEs (intraresidue, sequential, medium-range, and long-range) is provided in Figure 3. Helices D and A have more NOE restraints than other regions of the protein. Using these constraints and six distance restraints to a Ca^{2+} ion in site II, the structures of the ScNTnC·Ca^{2+} complex at 7 and 30 °C were calculated as described in Materials and Methods. The ensembles of 40 lowest-energy structures obtained at each temperature are shown in Figure 4.

The structural statistics are presented in Table 2. The quality of the ensemble solution structures was analyzed using Procheck (*30*). At 7 and 30 °C, 98.7 and 99.3% of the ϕ and ψ angles are in allowed regions of the Ramachandran plot, respectively. The remaining 1.3 or 0.7% is in the three unstructured residues in the N- and C-termini. There were no NOE violations greater than 0.2 Å.

The average volume and accessible surface area (ASA) for the ensemble of ScNTnC·Ca^{2+} structures at each temperature were calculated using Vadar (*29*), and are presented in Table 2. As the temperature increased, the volume and ASA both increased, by 250 Å^3 and 113 Å^2, respectively. The average distance between each atom and the center of mass of the protein increased by 0.08 Å, while the average distance between any two C_α atoms increased by 0.16 Å. These averages were calculated by measuring the distance from each atom to the calculated center of mass of the protein, and from each C_α to all other C_α atoms, with Insight II (Accelrys), and averaging the result. These distances were measured using the structure closest to average for each temperature.

At both temperatures, the ScNTnC·Ca^{2+} structure is typical of an EF-hand domain, with two helix−loop−helix motifs, and an N-terminal helix. The five helices correspond to residues 4−9 (N), 14−27 (A), 39−48 (B), 54−64 (C), and 74−84 (D). Residues from the EF-hand Ca^{2+}-binding loops (located between helices A and B and helices C and D) form an antiparallel β-sheet (residues 35−37 and 71−73). The interhelical angles and distances, as well as the degree of bending for each helix, were calculated with an in-house

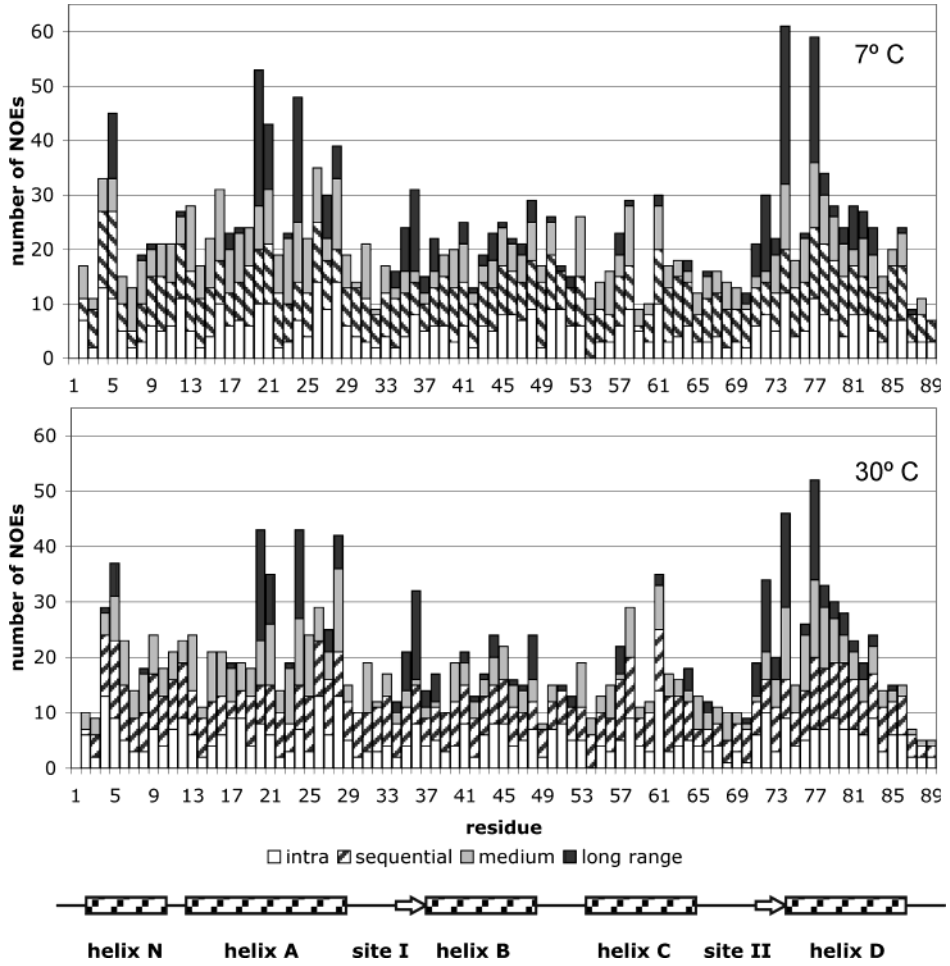

FIGURE 3: NOE restraint distribution at the two temperatures. The NOEs are divided among intraresidual (between two atoms in the same amino acid residue), shown in white, sequential (between atoms in neighboring residues), shown hatched, medium-range (between atoms that are two to four residues apart in the sequence), in gray, and long-range (between atoms that are more than four residues apart), in black.

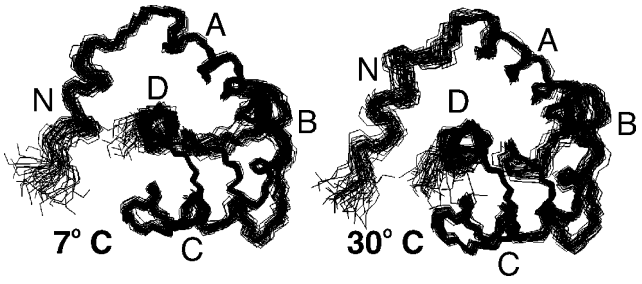

FIGURE 4: Ensembles of structures of the N-domain of trout cTnC, with one Ca^{2+} bound. Each ensemble has 40 structures. The five helices composing the protein are labeled as N (residues 4−9), A (residues 14−27), B (residues 39−48), C (residues 54−64), and D (residues 74−84). The structures are shown looking down at helix D. Both structures have the same overall fold; there are some differences in the relative position of the helices.

program written by S. M. Gagné, using all 40 structures for each temperature. The results are shown in Table 3. Helices A and B are slightly more bent at 7 °C than at 30 °C. With the decrease in temperature, helix D moves away from helix C and toward helices A and N, while helix N also moves slightly closer to helix A.

Backbone amide ^{15}N NMR relaxation data for the ScNTnC·Ca^{2+} complex at 600 MHz were analyzed for 75 residues at 30 °C and for 73 residues at 7 °C. The remaining residues could not be assigned or were overlapped in the $\{^1H,^{15}N\}$-HSQC spectra, or, for residues in the C-terminus, the peaks could not be seen in the proton-saturated $\{^1H\}-^{15}N$ NOE. The experimental backbone amide ^{15}N NMR relaxation values for the ScNTnC·Ca^{2+} complex at 7 and 30 °C are presented in Figure 5. The average T_1 values for all residues were 758 ± 44 at 7 °C and 501 ± 84 at 30 °C, while the average T_2 values for all residues were 85 ± 38 at 7 °C and 141 ± 42 at 30 °C. The average NOE was 0.73 ± 0.10 at 7 °C for all characterized residues and 0.66 ± 0.07 at 30 °C for all characterized residues except residue 89, which has an NOE of −1.15.

Low NOE values are an indication of significant internal motions of the backbone, on the picosecond to nanosecond time scale, that affect the measured T_1 and T_2 rates. At 600 MHz, this is usually considered true for residues with an NOE of <0.65. Residues 3, 30, 32, 33, 51, 86, and 87 have an NOE of <0.65 at 7 °C, while at 30 °C, this is true for residues 3, 4, 6−9, 11, 28−33, 39, 40, 51, 57, 63, 64, 83, 85, 86, and 89. Most of these residues are located in the N- and C-termini, in site I, or in the BC linker.

Backbone amide ^{15}N NMR relaxation data were interpreted using the Lipari−Szabo model-free approach, and the overall rotational tumbling was assumed to be isotropic. The overall correlation time (τ_m) for the ScNTnC·Ca^{2+} complex was determined from the T_1/T_2 ratio of residues falling within one standard deviation of the mean, excluding those residues

Table 3: Interhelical Angles and Distances[a]

	30 °C	7 °C
interhelical angle (deg)		
N−A	109 ± 5	96 ± 4
N−B	23 ± 8	54 ± 7
N−C	106 ± 10	93 ± 7
N−D	79 ± 10	103 ± 6
A−B	129 ± 3	136 ± 3
A−C	101 ± 5	117 ± 4
A−D	137 ± 4	128 ± 3
B−C	106 ± 3	98 ± 3
B−D	60 ± 2	51 ± 4
C−D	117 ± 4	110 ± 4
interhelical distance (Å)		
N−A	18.7 ± 0.4	17.7 ± 0.5
N−B	23.1 ± 0.6	22.5 ± 0.5
N−C	20.4 ± 0.6	20.1 ± 0.7
N−D	12.4 ± 0.4	10.5 ± 0.6
A−B	12.2 ± 0.2	12.3 ± 0.4
A−C	19.4 ± 0.3	19.5 ± 0.4
A−D	10.8 ± 0.2	10.2 ± 0.2
B−C	11.3 ± 0.4	11.3 ± 0.3
B−D	12.6 ± 0.4	12.9 ± 0.2
C−D	12.0 ± 0.3	12.7 ± 0.3
helix bends (deg)		
N	8 ± 2	3 ± 2
A	8 ± 4	19 ± 3
B	11 ± 3	19 ± 3
C	8 ± 3	9 ± 4
D	11 ± 2	10 ± 1

[a] Helix residues: 4−9 for helix N, 14−27 for helix A, 39−48 for helix B, 54−64 for helix C, and 74−84 for helix D.

with NOE values of <0.65, using an in-house Mathematica script (*32*). τ_m was found to be 5.0 ns at 30 °C and 9.4 ns at 7 °C.

The experimental relaxation parameters for each residue were fit to five motional models, using the Lipari−Szabo model-free analysis as implemented in TENSOR version 2.0 (*33*; see ref 32 for details of the calculation). The values of the order parameter S^2 obtained with the simplest model that fit each residue are plotted in Figure 6. The average S^2 values are 0.89 ± 0.03 at 30 °C and 0.90 ± 0.04 at 7 °C, for residues with an NOE of >0.65. The S^2 values indicate that the N- and C-termini, site I, and the BC linker are flexible on the picosecond to nanosecond time scale. The S^2 values at 7 and 30 °C are close to each other and show the same pattern according to the sequence, indicating a high degree of similarity of the dynamics of the ScNTnC·Ca^{2+} complex at the two temperatures.

DISCUSSION

The chemical shift changes of the H_α proton NMR resonance as the temperature decreases from 30 to 7 °C are all smaller than 0.05 ppm, while for the apo N-domain of skeletal TnC (sNTnC), larger changes were observed close to the N- and C-termini (*34*). The residues that change the most, between 0.04 and 0.05 ppm, are residues 5, 20, 46, and 82, with positive values, and residues 45 and 58, with negative values. This implies that residues 5, 20, 46, and 82 become slightly less helical with a decrease in temperature, while residues 45 and 58 become slightly more helical. Residues 5, 20, and 82 are located close to each other in the tertiary structure, as seen by the presence of NOE peaks, and the chemical shift changes may reflect changes in the distance between helices N, A, and D. The other three

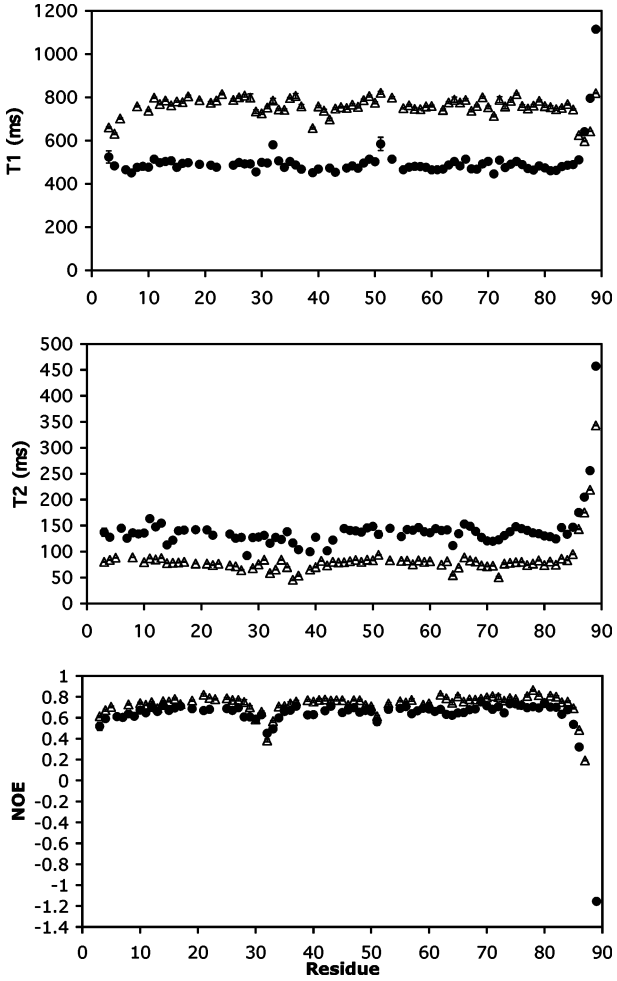

FIGURE 5: Backbone amide ^{15}N NMR relaxation times for the N-domain of trout cTnC, with one Ca^{2+} bound, at 7 (△) and 30 °C (●), at a magnetic field strength corresponding to a ^1H Larmor frequency of 600 MHz.

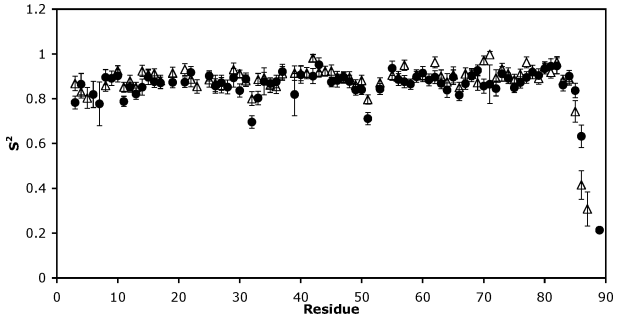

FIGURE 6: Backbone amide ^{15}N S^2 for the N-domain of trout cTnC, with one Ca^{2+} bound, at 7 (△) and 30 °C (●). S^2 was calculated under the assumption of isotropic tumbling.

residues are located in helices B and C. Overall, these changes occur in regions that would be affected by a change in the degree of opening of cTnC. In the apo N-domain of sNTnC, a number of chemical shift changes larger than 0.10 ppm were observed; the N- and C-termini showed negative changes as the temperature decreased, suggesting an increase of helicity, while residues 65 and 66 had positive changes (*34*). In the ScNTnC·Ca^{2+} complex, these regions exhibited small changes. The overall distribution of chemical shift changes in the ScNTnC·Ca^{2+} complex shows no correlation with apo-sNTnC, despite the similarity in structure. Residues that show a positive change in apo-sNTnC may have a

negative change in the ScNTnC·Ca^{2+} complex, and vice versa.

The ScNTnC·Ca^{2+} structure is somewhat better defined at 7 °C than at 30 °C, as can be seen in Figure 4. More NOEs were observed at 7 °C than at 30 °C, and this could be the reason for a better-defined structure at 7 °C. Alternatively, decreased molecular motions within the protein with the reduction in temperature can be the cause for both the increase in the number of observed NOEs and the better definition of the ScNTnC·Ca^{2+} structure at 7 °C. This effect of a better-defined NMR structure at a lower temperature was also seen when comparing lysozyme at 35 and 4 °C (*35*), and in skeletal apo-NTnC (*34*).

In both structures, the five helices were well-defined, with rmsds ranging from 0.31 (helix B at 30 °C) to 0.14 (helix N at 30 °C). The best-defined region of the ScNTnC·Ca^{2+} structure, at both temperatures, is the β-sheet formed by the two EF-hand sites, with rmsds of 0.11 at 30 °C and 0.12 at 7 °C. EF-hand site II, occupied by Ca^{2+}, is also well-defined (rmsd = 0.15 at 7 °C and 0.18 at 30 °C). EF-hand site I is not as well defined, with rmsds higher than those of the helices at the same temperature (0.41 at 7 °C and 0.33 at 30 °C). This is expected, since site I is empty and more flexible according to the order parameter S^2, and site II has the added distance restraints to the Ca^{2+} ion. Previous studies have shown that in mammalian cNTnC, site I is more flexible than site II (*21*, *36*).

The ScNTnC·Ca^{2+} structure is more expanded at 30 °C than at 7 °C, having a larger accessible surface area and volume (Table 2). Although this increase is close to the values of the standard deviation, it is accompanied by an increase in the distance between the C_α atoms, which supports the expansion of the protein. This increase in surface area and volume with an increase in temperature seems to be a general rule for proteins (*4*), and likely a direct consequence of changes in temperature. The same effect was detected in the NMR structures of skeletal apo-NTnC at 30 and 4 °C (*34*), lysozyme at 35 and 4 °C (*35*), and the spruce budworm antifreeze protein at 30 and 5 °C (*37*), and in crystal structures of myoglobin (*5*), trypsin (*8*), ribonuclease A (*9*), and lysozyme (*10*, *11*).

This expansion was first described by Frauenfelder and co-workers as an anisotropic expansion, in which the increase in the total volume does not come from an increase in the size of atom-sized internal cavities, but from an increase in the number of small packing imperfections between atoms (*5*). The average distance between pairs of atoms increases in the whole molecule, but some regions expand more than others. These small changes can combine themselves into larger changes, affecting the orientation of helices relative to each other. The same kind of expansion was described in other proteins (*8*−*11*).

In the ScNTnC·Ca^{2+} structure, a temperature increase of 23 °C caused the average distance from each atom to the center of mass to increase by 0.08 Å. This rate of expansion per degree Celsius is larger than those from any of the previously described proteins (*5*, *8*−*11*). Two factors probably contribute to that. In studies in which multiple temperatures over a wide range were examined, it was noticed that the thermal expansion is not linear with temperature (*10*, *11*). Since solution NMR does not permit the use of temperatures below freezing, we only looked at a small temperature range, close to the higher limit of temperature in the crystallographic studies. Thermal expansion is greater in the higher temperature ranges. Also, all the other studies were carried out by cooling protein crystals. The proteins in the crystal may not be as flexible or as capable of expansion as proteins in solution, considering that they are constrained by the crystalline arrangement.

The main difference between the structures at 7 and 30 °C, as seen in stereoview in Figure 7A, is the relative positioning of the helices. EF-hand domains can have two main conformations, "closed" and "open". The closed conformation is commonly found in apo EF-hand domains, while the open state is found when both EF-hand sites are bound to a metal ion; it is in this conformation that EF-hand domains interact with their targets. TnC domains follow this general rule. The N-terminal domain of cardiac TnC, however, has only one functional EF-hand site, and stays closed in the presence of calcium, only moving to the open state in the presence of troponin I (TnI). The ScNTnC·Ca^{2+} structures at 7 and 30 °C are very similar to each other and to the structure of the N-terminal domain of mammalian cTnC with one Ca^{2+} bound, being also closed TnC structures.

When a TnC domain opens with the binding of Ca^{2+} or troponin I (TnI), there is a relative movement between helices B and C (forming the structural unit BC), on one side, and N, A, and D (structural unit NAD), on the other side. To compare the degree of opening of the ScNTnC·Ca^{2+} structure at the two different temperatures, structures at the two different temperatures were superimposed using the structural unit BC. The structure closest to the average in each of the two structural ensembles was used for this superimposition (Figure 7A).

The classical parameters for the opening and closing of a TnC domain are changes in the angles between helices A and B and helices C and D (*38*). The angle between helices C and D does not change in the ScNTnC·Ca^{2+} structure, and the angle between helices A and B increases as the temperature decreases. The other interhelical angle changes, however (helices N and B, B and C, and B and D), happen in the same direction as in the classic opening example, skeletal TnC upon Ca^{2+} binding (*38*). All the interhelical angle changes are much smaller than those that occur in skeletal TnC. Overall, these changes result in a slightly more open structure at 7 °C than at 30 °C.

The differences in the angle and distance of the helices between the structures at 7 and 30 °C can be related to smaller changes within the protein. Changes in the EF-hand loop I are reflected in the position of helix N. Helices A and B are more bent at 7 °C than at 30 °C (Table 3). The bending of helix A causes a change in the distance from helices N and D to A, and in the interhelical angles between helix A and all the other helices, while the bending of helix B causes the changes in the interhelical angles between helix B and all other helices.

ScNTnC·Ca^{2+} structures were compared to other closed structures (all determined at 30 °C), such as mammalian apo-cNTnC and apo-sNTnC, mammalian cNTnC·Ca^{2+}, and the skeletal NTnC mutant E41A, which had the glutamate in position 12 of site I replaced with an alanine, reducing the affinity of site I for Ca^{2+} (*18*). E41A has two EF-hand Ca^{2+}-binding sites, one in the micromolar range (site II) and one

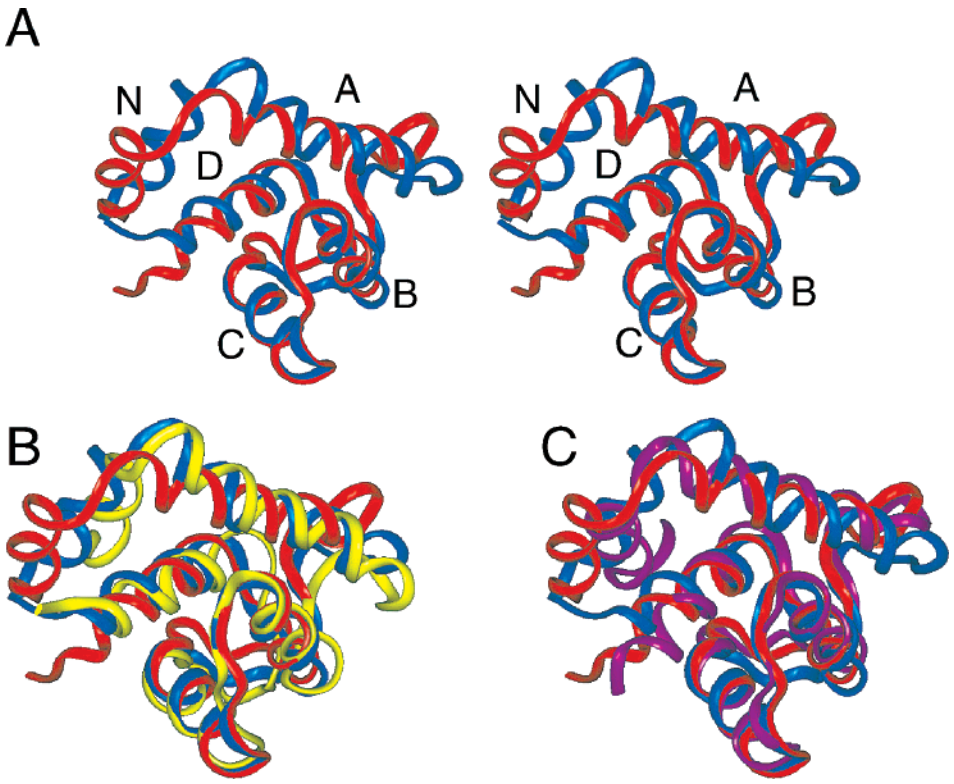

FIGURE 7: Superimposition of the structures of trout and mammalian cNTnC and E41A sNTnC. (A) Stereoview of the superimposition of one-Ca^{2+} trout cNTnC (ScNTnC·Ca^{2+}) at 7 and 30 °C: red for 30 °C and blue for 7 °C. (B) ScNTnC·Ca^{2+} at 7 and 30 °C and mammalian cNTnC·Ca^{2+}: red for ScNTnC·Ca^{2+} at 30 °C, blue for ScNTnC·Ca^{2+} at 7 °C, and yellow for mammalian cNTnC·Ca^{2+} (*20*). (C) ScNTnC·Ca^{2+} at 7 and 30 °C and the skeletal E41A NTnC mutant: red for ScNTnC·Ca^{2+} at 30 °C, blue for ScNTnC·Ca^{2+} at 7 °C, and purple for the E41A sNTnC·Ca^{2+} mutant (*18*). The structures were superimposed by helices B and C, to evaluate the opening of the domain. All the helices are labeled in panel A; the same view is presented in panels B and C. ScNTnC·Ca^{2+} has a slightly more open structure at 7 °C than at 30 °C. ScNTnC·Ca^{2+} at 7 °C is more similar to mammalian cNTnC·Ca^{2+}, while ScNTnC·Ca^{2+} at 30 °C is more similar to the E41A sNTnC·Ca^{2+} mutant.

in the millimolar (site I) range, much like ScNTnC. Despite binding two Ca^{2+} ions, E41A does not open, and its structure is similar to the ScNTnC·Ca^{2+} structure at 30 °C. This raises the possibility that the conformation of TnC is closely related to the binding properties of each isoform. It is not known if ScNTnC would adopt an open or closed conformation when bound to two Ca^{2+} ions.

The ScNTnC·Ca^{2+} structure at 7 °C and the mammalian cNTnC·Ca^{2+} structure at 30 °C (*20*) show the greatest similarity (rmsd = 1.76, Figure 7B) at their respective physiological temperatures, suggesting that there is an optimal functional conformation of cTnC for the regulation of muscle contraction. This is a higher level of similarity than between the two ScNTnC·Ca^{2+} structures (rmsd = 1.94). At 30 °C, the degree of similarity is greater with the E41A·2Ca^{2+} structure (*18*) (rmsd = 1.98, Figure 7C), which has similar binding properties, than with the mammalian cNTnC·Ca^{2+} structure, whose sequence is much more homologous. Three amino acid differences between mammalian cNTnC·Ca^{2+} and ScNTnC·Ca^{2+} sequences in site I (positions 28−30) are likely the main reason for their structure differences. The two other amino acid differences are conservative, and not likely to affect the structure.

The accessible surface area (ASA) of the ScNTnC·Ca^{2+} structure at 7 °C is also more similar to the ASA of mammalian cNTnC (6047 Å). The exposed surface area is extremely important for interactions with other proteins; therefore, it is to be expected that homologues that work at different temperatures have adaptations to ensure that the exposed surface remains the same at their respective physiological temperatures.

When the backbone dynamics properties of ScNTnC·Ca^{2+} are compared to those of mammalian cNTnC, the similarity is also evident. As with structures, the dynamic properties of Ca^{2+}-bound mammalian cNTnC have not been studied at 7 °C. The analysis of backbone amide ^{15}N NMR relaxation data of apo and Ca^{2+}-bound mammalian cNTnC at 30 °C (*21*) and of mammalian apo-cNTnC at various temperatures ranging from 5 to 45 °C (*36*), however, offers interesting material for comparison. The τ_m values at 30 °C are identical for ScNTnC·Ca^{2+} and for mammalian cNTnC·Ca^{2+} complexes (5 ns), while mammalian apo-cNTnC has a slightly higher τ_m (5.4 ns). As the temperature decreases, the τ_m values for both ScNTnC·Ca^{2+} and mammalian apo-cNTnC increased 4%/°C to 9.4 and 10.6 ns, respectively, consistent with the Stokes−Einstein equation ($\tau_m \propto \eta/T$).

The three backbone amide ^{15}N NMR relaxation parameters (T_1, T_2, and NOE) and the order parameter S^2 show, at both temperatures, the same patterns observed for the mammalian isoform of cNTnC in the presence of Ca^{2+} (*21*), with greater flexibility in the N- and C-termini, site I, and the BC linker. S^2 values suggest that helix N is slightly more flexible than the other helices, as observed for the mammalian cNTnC·Ca^{2+} complex. Overall, the different properties of the ScNTnC·Ca^{2+} complex at the two temperatures and when compared to the mammalian cNTnC·Ca^{2+} complex cannot be explained by backbone dynamics on the picosecond to nanosecond time scale.

The comparison of ScNTnC·Ca^{2+} structures at the two different temperatures, 7 and 30 °C, shows effects of temperature that are also seen in other proteins whose structures were determined at different temperatures, such as a more compact structure at lower temperatures. The comparison of ScNTnC·Ca^{2+} structures with other closed TnC structures shows evidence of thermal adaptation to the colder and more variable physiological temperatures in trout. In this way, the smaller changes in H_α may indicate that the secondary structure of the ScNTnC·Ca^{2+} complex changes less with the change in temperature than that of mammalian apo-cNTnC. This may be consistent with an organism that lives in a wider temperature range. The backbone conformation and exposed surface are most similar between the ScNTnC·Ca^{2+} structure at 7 °C and mammalian cNTnC at 30 °C, suggesting that different isoforms of proteins in general would have the same optimal functional conformation and exposed surface at their respective physiological temperatures.

ACKNOWLEDGMENT

We thank Dr. Pascal Mercier for the help in the analysis of the relaxation data and Dr. Carolyn Slupsky for her help with the structural calculations. We also thank Mr. Gerry McQuaid for keeping the spectrometers always in excellent condition. We acknowledge the Canadian National High Field NMR Centre (NANUC) for their assistance and use of the facilities. Operation of NANUC is funded by the Canadian Institutes of Health Research (CIHR), the Natural Science and Engineering Research Council of Canada (NSERC), and the University of Alberta.

REFERENCES

1. D'Amico, S., Claverie, P., Collins, T., Georlette, D., Gratia, E., Hoyoux, A., Meuwis, M.-A., Feller, G., and Gerday, C. (2002) *Philos. Trans. R. Soc. London, Ser. B 357*, 917−925.
2. Rees, D. C., and Robertson, A. D. (2001) *Protein Sci. 10*, 1187−1194.
3. Kundrot, C. E., and Richards, F. M. (1987) *J. Mol. Biol. 193*, 157−170.
4. Gekko, K., and Hasegawa, Y. (1989) *J. Phys. Chem. 93*, 426−429.
5. Frauenfelder, H., Hartmann, H., Karplus, M., Kuntz, I. D., Jr., Kuriyan, J., Parak, F., Petsko, G. A., Ringe, D., Tilton, R. F., Jr., Connolly, M. L., and Max, N. (1987) *Biochemistry 26*, 254−261.
6. Iqbal, M., and Verrall, R. E. (1987) *J. Phys. Chem. 91*, 1935−1941.
7. Palma, R., and Curmi, P. M. G. (1999) *Protein Sci. 8*, 913−920.
8. Earnest, T., Fauman, E., Craik, C. S., and Stroud, R. (1991) *Proteins 10*, 171−187.
9. Tilton, R. F., Jr., Dewan, J. C., and Petsko, G. A. (1992) *Biochemistry 31*, 2469−2481.
10. Young, A. C. M., Tilton, R. F., and Dewan, J. C. (1994) *J. Mol. Biol. 235*, 302−317.
11. Kurinov, I. V., and Harrison, R. W. (1995) *Acta Crystallogr. D51*, 98−109.
12. Harrison, S. M., and Bers, D. M. (1990) *Am. J. Physiol. 258*, C282−C288.
13. Gillis, T. E., Marshall, C. R., Xue, X. H., Borgford, T. J., and Tibbits, G. F. (2000) *Am. J. Physiol. 279*, R1701−R1715.
14. Zot, A. S., and Potter, J. D. (1987) *Annu. Rev. Biophys. Biophys. Chem. 16*, 535−559.
15. Lewit-Bentley, A., and Réty, S. (2000) *Curr. Opin. Struct. Biol. 10*, 637−643.
16. van Eerd, J.-P., and Takahashi, K. (1975) *Biochem. Biophys. Res. Commun. 64*, 122−127.
17. Gillis, T. E., Blumenschein, T. M. A., Sykes, B. D., and Tibbits, G. F. (2003) *Biochemistry 42*, 6418−6426.
18. Gagné, S. M., Li, M. X., and Sykes, B. D. (1997) *Biochemistry 36*, 4386−4392.
19. Gillis, T. E., Moyes, C. D., and Tibbits, G. F. (2003) *Am. J. Physiol. 284*, C1176−C1184.
20. Spyracopoulos, L., Li, M. X., Sia, S. K., Gagné, S. M., Chandra, M., Solaro, R. J., and Sykes, B. D. (1997) *Biochemistry 36*, 12138−12146.
21. Spyracopoulos, L., Gagné, S. M., Li, M. X., and Sykes, B. D. (1998) *Biochemistry 37*, 18032−18044.
22. Delaglio, F., Grzwsiek, S., Vuister, G. W., Zhu, G., Pfeifer, J., and Bax, A. (1995) *J. Biomol. NMR 6*, 277−293.
23. Johnson, B., and Blevins, R. (1994) *J. Biomol. NMR 4*, 603−614.
24. Kuboniwa, H., Grzwsiek, S., Delaglio, F., and Bax, A. (1994) *J. Biomol. NMR 4*, 871−878.
25. Gagné, S. M., Tsuda, S., Li, M. X., Chandra, M., Smillie, L. B., and Sykes, B. D. (1994) *Protein Sci. 3*, 1961−1974.
26. Archer, S. J., Ikura, N. I., Torchia, D. A., and Bax, A. (1991) *J. Magn. Reson. 95*, 636−641.
27. Brünger, A. T. (1992) *X-PLOR, Version 3.1 A System for X-ray Crystallography and NMR*, Yale University Press, New Haven, CT.
28. Strynadka, N. C., and James, M. N. G. (1989) *Annu. Rev. Biochem. 58*, 951−998.
29. Willard, L., Ranjan, A., Zhang, H., Monzavi, H., Boyko, R. F., Sykes, B. D., and Wishart, D. S. (2003) *Nucleic Acids Res. 31*, 3316−3319.
30. Laskowski, R. A., MacArthur, M. W., Moss, D. S., and Thornton, J. M. (1993) *J. Appl. Crystallogr. 26*, 283−290.
31. Farrow, N. A., Muhandiram, R., Singer, A. U., Pascal, S. M., Kay, C. M., Gish, G., Shoelson, S. E., Pawson, T., Forman-Kay, J. D., and Kay, L. E. (1994) *Biochemistry 33*, 5984−6003.
32. Mercier, P., Spyracopoulos, L., and Sykes, B. D. (2001) *Biochemistry 40*, 10063−10077.
33. Dosset, P., Hus, J.-C., Blackledge, M., and Marion, D. (2000) *J. Biomol. NMR 16*, 23−28.
34. Tsuda, S., Miura, A., Gagné, S. M., Spyracopoulos, L., and Sykes, B. D. (1999) *Biochemistry 38*, 5693−5700.
35. Kumeta, H., Miura, A., Kobashigawa, Y., Miura, K., Oka, C., Nemoto, N., Nitta, K., and Tsuda, S. (2003) *Biochemistry 42*, 1209−1216.
36. Spyracopoulos, L., Lavigne, P., Crump, M. P., Gagné, S. M., Kay, C. M., and Sykes, B. D. (2001) *Biochemistry 40*, 12541−12551.
37. Graether, S. P., Gagné, S. M., Spyracopoulos, L., Jia, Z., Davies, P. L., and Sykes, B. D. (2003) *J. Mol. Biol. 327*, 1155−1168.
38. Gagné, S. M., Tsuda, S., Li, M. X., Smillie, L. B., and Sykes, B. D. (1995) *Nat. Struct. Biol. 2*, 784−789.
39. Kay, L. E., Keifer, P., and Saarinen, T. (1992) *J. Am. Chem. Soc. 114*, 10663−10665.
40. Zhang, O., Kay, L. E., Olivier, J. P., and Forman-Kay, J. D. (1994) *J. Biomol. NMR 4*, 845−858.
41. Macura, S., and Ernst, R. R. (1980) *Mol. Phys. 41*, 95−117.

BI035504Z